

Comparison of Active Constrained Layer Damping by Using Extension and Shear Mode Piezoceramic Actuators

R. C. BATRA* AND T. S. GENG

*Department of Engineering Science and Mechanics, M/C 0219, Virginia Polytechnic Institute and State University
Blacksburg, VA 24061, USA*

ABSTRACT: We analyze, numerically by the finite element method, three-dimensional electromechanical deformations of a thick laminated plate with layers made of aluminum, a viscoelastic material and a piezoceramic (PZT). Two arrangements of layers are considered. In one case a central PZT layer is surrounded on both sides by viscoelastic layers and aluminum layers are on the outside surfaces. The PZT is poled in the longitudinal direction and an electric field is applied to it in the transverse direction. Thus shearing deformations of the PZT layer dominate over its extensional deformations. In the second arrangement, the aluminum layer is in the middle and the PZT layers are on the outside. The poling direction and the electric field are along the thickness of the PZT layer. Extensional deformations of the PZT layer are significantly more than its shearing deformations. The problem formulation incorporates geometric nonlinearities and the constitutive relation for the PZT includes quadratic terms in the electric field. For each set up of the layers, the system is excited at its first natural frequency. The enhancement in damping induced by the actuation of the PZT layers is ascertained, and the optimum thicknesses of the viscoelastic layers and the PZT layers for maximum damping are determined. The effect of nonlinear terms in the constitutive relation for the PZT is ascertained. The problem of exciting the laminated plate simultaneously at the first and the second frequencies and annulling these has been scrutinized. It is found that the energy of electric deformations of the PZT material is more for the shear mode actuators than that for the extension mode actuators.

Key Words: thick laminated plates, viscoelasticity, piezoelectricity, three-dimensional deformations, functionally graded viscoelastic layer, finite element solution

INTRODUCTION

SEVERAL investigators (e.g., Plump and Hubbard, 1986; Edberg and Bicos, 1992; Azvine et al., 1994; Van Nostrand et al., 1994; Baz, 1993; Baz and Ro, 1993a,b, 1995a,b; Shen, 1994) have analyzed active constrained layer damping (ACLD) treatments for quickly annulling vibrations of a structure. The energy dissipated per unit volume of the viscoelastic material is usually higher in the ACLD treatment than that in the passive constrained layer damping (PCLD) treatment. Usually an ACLD treatment consists of a viscoelastic layer with one face bonded to the host structure and the other to a piezoceramic (PZT)¹ layer. Deformations of the PZT layer are controlled by applying a suitable voltage difference across its faces which in turn enhances shear deformations of the viscoelastic layer. In a PCLD treatment, there is no actuator to enhance shearing deformations of the viscoelastic layer either embedded

in the host structure or bonded to its outer surface. Ideally, the damping treatment should dissipate energy efficiently but not noticeably alter the dynamic characteristics of the host structure.

We note that Van Nostrand et al. (1994) concluded that active actions will be degraded by the passive constraining layer. Bailey et al. (1988) stated that it is more effective to apply piezoelectric materials directly on the structure rather than embed a viscoelastic layer between the two. Liao and Wang (1997a) have shown that a viscoelastic layer reduces the transmissibility and hence the direct control authority from the active source to the host structure. They (1997b) have identified ranges of viscoelastic material properties which will provide satisfactory transmissibility of active actions, and the overall performance will exceed that of purely passive and active systems.

Previous studies of ACLD treatments have employed extension mode PZT actuators in which the electric field and the poling direction are along the thickness of the PZT layer. The thickness of the PZT changes and the transverse displacements induced due to the Poisson

*Author to whom correspondence should be addressed.

E-mail: rbatra@vt.edu

¹The abbreviation PZT is used to denote a generic piezoceramic rather than a specific one.

effect in the PZT increase shear deformations of the viscoelastic layer. Alternatively, one could exploit shear mode deformations of the PZT in which it is poled in a longitudinal direction and the electric field is applied across its thickness. Note that different piezoelectric constants are effective in the extension and in the shear mode actuation. Shear mode PZTs are commercially available². Closed-form solutions for shear mode PZT beams were given by Boriseiko et al. (1983). They were studied by Sun and Zhang (1996) and Zhang and Sun (1999) for controlling deformations of a laminated structure. Vel and Batra (2001a,b) have given exact solutions for static deformations of simply supported laminated structures incorporating shear mode actuators. Here we compare their effectiveness in ACLD treatments with that of extension mode actuators. As pointed out by Sun and Zhang (1996) and verified by the analytical solutions of Vel and Batra (2001a,b), an advantage of shear mode actuators is that for the same tip deflection the maximum bending stress induced in them is less than that in the extension mode actuators. Also, they are embedded within the structure and hence are not exposed to environmental effects.

Analysis of dynamic problems involving ACLD treatments requires a mathematical model (i.e., governing equations, and initial and boundary conditions) of the system. Such problems have been studied by the finite element method (e.g., see Van Nostrand et al. 1994; Baz and Ro, 1993a, 1993b; Shi et al., 2001) or by distributed-parameter methods (e.g., see Plump and Hubbard, 1986; Baz, 1993; Shen, 1994; Azvine et al., 1994; Baz and Ro, 1993, 1995) which employ shear models of Mead and Markus (1969) and DiTaranto (1965). Nearly all of these studies are limited to beam like structures and therefore make kinematic assumptions of the beam theory.

We note that Yu (1995) has used a pseudo variational principle to derive equations of motion of piezoelectricity and specialized these to a plate. These equations incorporate von Kármán's geometric nonlinearities and employ linear constitutive relations. Tzou and Bao (1997) have also considered von Kármán's geometric nonlinearities, linear constitutive relations and used the Hamilton principle to derive governing equations for a thermopiezoelectric shell. On the contrary we study here three-dimensional deformations of very thick clamped plates/beams and account for geometric nonlinearities. Furthermore, the constitutive relation for the PZT has second-order terms in the electric field to incorporate nonlinear dependence of strains upon the electric field observed by Crawley and Anderson (1990). However, temperature dependence of the material properties and heat generated due to viscous dissipation and the electric field have not been considered. Thus the temperature is

assumed to be constant throughout the deformation process.

FORMULATION OF THE PROBLEM

A schematic sketch of the problem studied is shown in Figure 1(a) and (b); Figure 1(a) depicts an ACLD treatment with a shear mode PZT actuator and Figure 1(b) with two extension mode PZT actuators. The total thicknesses of the PZT and the aluminum layers in the two cases are the same. However, because of the differences in the vertical positions of the two layers and in their material properties, their structural stiffnesses will be different. Thus the same load applied at geometrically similar points will result in different deformations of points in the aluminum layers. Whereas the electric field is applied in the x_3 -direction for both the shear mode and the extension mode PZT actuators, they are poled in the x_1 -direction in the former case and in the x_3 -direction in the latter case.

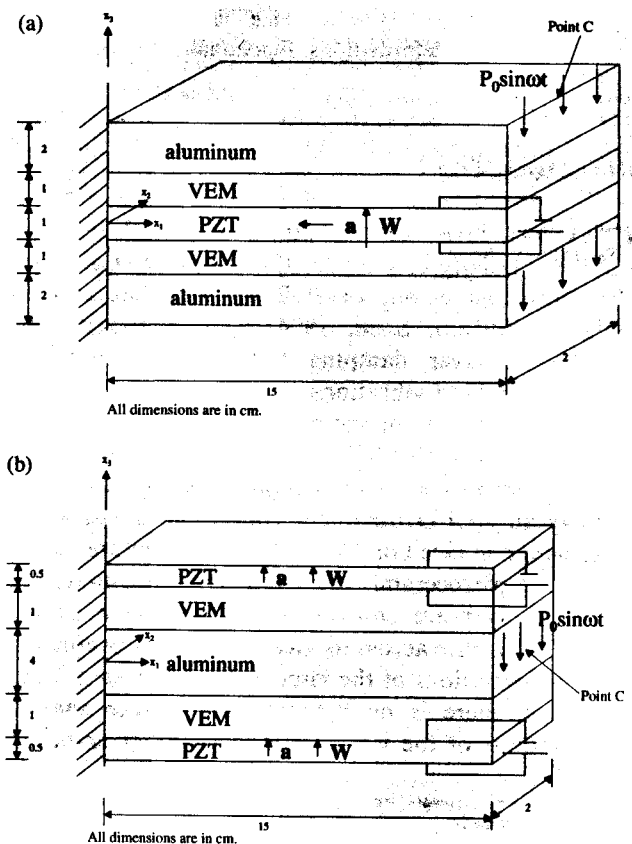


Figure 1. Schematic sketch of the problem studied: (a) ACLD treatment with a shear mode actuator; (b) ACLD treatment with extension mode actuators. Unit vectors \mathbf{a} and \mathbf{W} point in the directions of polarization and the electric field respectively.

²Electro Ceramic Div., Morgan Matroc, Bedford, OH.

In the Lagrangean description of motion and in the absence of body forces and distributed charges, equations governing dynamic deformations of a structure are

$$\rho J = \rho_0, \quad (1)$$

$$\rho_0 \dot{x}_i = T_{i\alpha, \alpha}, \quad i = 1, 2, 3, \quad \alpha = 2, 3, \quad (2)$$

$$T_{i\alpha} x_{j, \alpha} = T_{j\alpha} x_{i, \alpha}, \quad (3)$$

$$D_{\alpha, \alpha} = 0, \quad (4)$$

where we have used rectangular Cartesian coordinates x_i and X_α to describe the position of the same material particle in the present and the reference configurations respectively. A superimposed dot indicates the material time derivative, $J = \det[x_{i, \alpha}]$, $F_{i\alpha} = x_{i, \alpha} \equiv \partial x_i / \partial X_\alpha$ is the deformation gradient, \mathbf{T} is the first Piola–Kirchhoff (or the nominal or the engineering) stress tensor, a repeated index implies summation over the range of the index, ρ and ρ_0 equal mass densities in the present and the reference configurations respectively, and \mathbf{D} is the electric displacement. Latin and Greek indices signify components of a tensor with respect to coordinates in the present and the reference configurations respectively. Equations (1)–(4) express, respectively, the balance of mass, the balance of linear momentum, the balance of moment of momentum, and the Maxwell equation with inertia effects associated with the electric field neglected. Note that the balance of moment of momentum is identically satisfied by requiring that the Cauchy stress tensor, $\boldsymbol{\sigma}$, related to \mathbf{T} by

$$\sigma_{ij} = J^{-1} T_{i\alpha} x_{j, \alpha} = J^{-1} T_{i\alpha} F_{j\alpha}, \quad (5)$$

be symmetric. Furthermore, once the present positions x_i of material particles are known, the present mass density can be computed from Equation (1). Thus we need to solve Equations (2) and (4) for x_i and the electric potential. Equations (2) and (4) are to be supplemented by initial and boundary conditions and constitutive relations.

We assume that the host structure and the viscoelastic layer are made of homogeneous and isotropic materials and the PZT of a homogeneous and transversely isotropic material with the axis of transverse isotropy coincident with the poling direction. In terms of the symmetric second Piola–Kirchhoff stress tensor, $\mathbf{S}_{\alpha\beta}$, related to the first Piola–Kirchhoff stress tensor \mathbf{T} by

$$T_{i\alpha} = x_{i, \beta} S_{\alpha\beta} = F_{i\beta} S_{\alpha\beta}, \quad (6)$$

constitutive relations for materials of the three layers are given below.

Host layer:

$$S_{\alpha\beta} = \frac{\nu Y}{(1+\nu)(1-2\nu)} E_{\gamma\gamma} \delta_{\alpha\beta} + \frac{Y}{(1+\nu)} E_{\alpha\beta}; \quad (7)$$

Viscoelastic material:

$$S_{\alpha\beta} = \frac{\nu Y \delta_{\alpha\beta}}{(1+\nu)(1-2\nu)} \left[E_{\gamma\gamma}(t) - \frac{\chi}{\tau} \int_{-\infty}^t e^{-(t-s)/\tau} E_{\gamma\gamma}(s) ds \right] + \frac{Y}{(1+\nu)} \left[E_{\alpha\beta}(t) - \frac{\chi}{\tau} \int_{-\infty}^t e^{-(t-s)/\tau} E_{\alpha\beta}(s) ds \right]; \quad (8)$$

PZT:

$$\begin{aligned} \mathbf{S} = & (2c_1 I_1 + c_3 I_2 + e_1 I_3 + 3\lambda_1 I_1^2 + 2\lambda_3 I_1 I_2 + \lambda_4 I_2^2 \\ & + \lambda_5 II_1 + \lambda_7 II_2 + 2\nu_1 I_1 I_3 + \nu_2 I_3^2 + \nu_7 II_3 + \nu_9 II_4 \\ & + \nu_{14} I_2 I_3) \mathbf{a} \otimes \mathbf{a} + (2c_2 I_2 + c_3 I_1 + e_2 I_3 + 3\lambda_2 I_2^2 + \lambda_3 I_1^2 \\ & + 2\lambda_4 I_1 I_2 + \lambda_6 II_1 + \lambda_8 II_2 + 2\nu_3 I_2 I_3 + \nu_4 I_3^2 + \nu_8 II_3 \\ & + \nu_{10} II_4 + \nu_{14} I_1 I_3) \mathbf{1} \\ & + (c_4 + \lambda_5 I_1 + \lambda_6 I_2 + \nu_5 I_3) (\mathbf{a} \otimes \mathbf{E} \cdot \mathbf{a} + \mathbf{a} \cdot \mathbf{E} \otimes \mathbf{a}) \\ & + 2(c_5 + \lambda_7 I_1 + \lambda_8 I_2 + \nu_6 I_3) \mathbf{E} \\ & + (e_3 + \nu_9 I_1 + \nu_{10} I_2 + \nu_{11} I_3) (\mathbf{a} \otimes \mathbf{W} + \mathbf{W} \otimes \mathbf{a}) \\ & + 3\lambda_9 \mathbf{E}^2 + \nu_{12} \mathbf{W} \otimes \mathbf{W} + \nu_{13} (\mathbf{a} \otimes \mathbf{E} \cdot \mathbf{W} + \mathbf{W} \cdot \mathbf{E} \otimes \mathbf{a} \\ & + \mathbf{W} \otimes \mathbf{E} \cdot \mathbf{a} + \mathbf{a} \cdot \mathbf{E} \otimes \mathbf{W}), \\ \boldsymbol{\pi} = & (2\epsilon_1 I_3 + e_1 I_1 + e_2 I_2 + 3\mu_1 I_3^2 + \mu_2 II_3 + \nu_1 I_1^2 \\ & + 2\nu_2 I_3 I_1 + \nu_3 I_2^2 + 2\nu_4 I_3 I_2 + \nu_5 II_1 + \nu_6 II_2 + \nu_{11} II_4 \\ & + \nu_{14} I_1 I_2) \mathbf{a} + 2(\epsilon_2 + \mu_2 I_3 + \nu_7 I_1 + \nu_8 I_2) \mathbf{W} \\ & + 2(e_3 + \nu_9 I_1 + \nu_{10} I_2 + \nu_{11} I_3) \mathbf{E} \cdot \mathbf{a} \\ & + 2\nu_{12} \mathbf{E} \cdot \mathbf{W} + 2\nu_{13} \mathbf{E}^2 \cdot \mathbf{a}; \end{aligned} \quad (9)$$

where

$$\begin{aligned} E_{\alpha\beta} = & (u_{\alpha, \beta} + u_{\beta, \alpha} + u_{\gamma, \alpha} u_{\gamma, \beta}) / 2, \\ u_\alpha = & x_i \delta_{i\alpha} - X_\alpha; \end{aligned} \quad (10)$$

$$\begin{aligned} I_1 = & \mathbf{a} \cdot \mathbf{E} \mathbf{a}, \quad I_2 = \text{tr } \mathbf{E}, \quad I_3 = \mathbf{a} \cdot \mathbf{W}, \\ II_1 = & \mathbf{a} \cdot \mathbf{E}^2 \mathbf{a}, \quad II_2 = \text{tr } \mathbf{E}^2, \quad II_3 = \mathbf{W} \cdot \mathbf{W}, \\ II_4 = & \mathbf{a} \cdot \mathbf{E} \mathbf{W} + \mathbf{W} \cdot \mathbf{E} \mathbf{a}. \end{aligned} \quad (11)$$

Here \mathbf{u} equals the mechanical displacement of a material point, \mathbf{E} is the Green–St. Venant strain tensor appropriate for finite deformations of a body, $\delta_{\alpha\beta}$ is the Kronecker delta, \mathbf{a} is a unit vector along the poling direction of the PZT, $\mathbf{b} \otimes \mathbf{c}$ denotes the tensor product between vectors \mathbf{b} and \mathbf{c} defined as $(\mathbf{b} \otimes \mathbf{c}) \mathbf{d} = (\mathbf{c} \cdot \mathbf{d}) \mathbf{b}$ for every vector \mathbf{d} , $\mathbf{b} \cdot \mathbf{c}$ denotes the inner product between vectors \mathbf{b} and \mathbf{c} , $\boldsymbol{\pi}$ is the polarization vector that is related to the electric displacement \mathbf{D} , the electric field \mathbf{W} and the electric potential ϕ through

$$\pi_\alpha = D_\alpha - \epsilon_0 J X_{\alpha, i} X_{\beta, i} W_\beta, \quad W_\beta = -\phi_{, \beta}.$$

where ϵ_0 is the dielectric permittivity of the free space.

In Equation (7) Y is Young's modulus and ν Poisson's ratio. Equation (7) implies that the material of the host

layer is being modeled as neo-Hookean. Equation (8) signifies that both the shear and the bulk response of the viscoelastic material have the same relaxation time τ and the Poisson ratio is independent of time. If relaxation times and/or values of χ for the bulk and the shear moduli are different, then Poisson's ratio of the viscoelastic material will depend upon time t . Also, generalization to the case of more than one relaxation time for the shear and the bulk moduli is fairly straight forward to implement in the analysis of the problem. Christensen (1971) has discussed how Equation (8) relates to nonlinear viscoelastic materials; here we note that it is analogous to Equation (7). Yu and Batra (2000) used the analogue of Equation (8) for incompressible materials to analyze damping induced by a viscoelastic layer enclosed between two cylinders and undergoing finite torsional deformations. For the strain history

$$\mathbf{E}(t) = \mathbf{E}^0, \quad (13)$$

Equation (8) yields

$$S_{\alpha\beta} = \left(\frac{\nu Y}{(1+\nu)(1-2\nu)} E_{\gamma\gamma}^0 \delta_{\alpha\beta} + \frac{Y}{(1+\nu)} E_{\alpha\beta}^0 \right) (1 - \chi + \chi e^{-t/\tau}).$$

Thus the stress eventually relaxes to $(1 - \chi)$ times that in a neo-Hookean material with Young's modulus Y and Poisson's ratio ν .

For infinitesimal sinusoidal deformations with the strain history

$$E_{\alpha\beta}(t) = \varepsilon_{\alpha\beta}^0 \sin \omega t, \quad |\varepsilon_{\alpha\beta}^0| \ll 1 \quad (15)$$

Equation (8) gives

$$S_{\alpha\beta}(t) = \frac{((1 + \tau^2 \omega^2 - \chi)^2 + \chi^2 \tau^2 \omega^2)^{1/2}}{1 + \omega^2 \tau^2} \times \left[\frac{\nu Y \varepsilon_{\gamma\gamma}^0}{(1+\nu)(1-2\nu)} \delta_{\alpha\beta} + \frac{Y}{1+\nu} \varepsilon_{\alpha\beta}^0 \right] \sin(\omega t + \delta),$$

where

$$\tan \delta = (\chi \omega \tau) / (1 + \tau^2 \omega^2 - \chi). \quad (17)$$

Thus the phase shift, δ , between the applied infinitesimal sinusoidal strain history and the induced stress history depends upon the frequency ω , the relaxation time τ and the factor χ . Also, the amplitude of each component of stress is smaller than $(1 + \chi^2)^{1/2}$ times that in a Hookean material of Young's modulus Y and Poisson's ratio ν . Each component of stress exhibits the same phase shift with respect to its value in the corresponding Hookean material for which $\chi = 0$. The storage bulk and shear moduli of the viscoelastic material equal $(1 - \chi / (1 + \tau^2 \omega^2))$ times those for the corresponding elastic

material, and the multiplying factor for the loss moduli is $\chi \omega \tau / (1 + \omega^2 \tau^2)$. Thus the maximum value of the loss moduli and hence of energy dissipated per unit volume of the viscoelastic material occurs for $\tau = 1/\omega$. It is not easy to identify the storage and the loss moduli in the presence of geometric nonlinearities.

With the definition

$$\eta_{\alpha\beta}(t) = \frac{1}{\tau} \int_{-\infty}^t e^{-(t-s)/\tau} E_{\alpha\beta}(s) ds, \quad (18)$$

Equation (8) becomes

$$S_{\alpha\beta} = \left(\frac{\nu Y (1 - \chi)}{(1 + \nu)(1 - 2\nu)} \eta_{\gamma\gamma} \delta_{\alpha\beta} + \frac{Y (1 - \chi)}{(1 + \nu)} \eta_{\alpha\beta} \right) + \frac{\nu Y \tau}{(1 + \nu)(1 - 2\nu)} \dot{\eta}_{\gamma\gamma} \delta_{\alpha\beta} + \frac{Y \tau}{(1 + \nu)} \dot{\eta}_{\alpha\beta}. \quad (19)$$

With $\eta_{\alpha\beta}$ interpreted as a pseudo strain and $\dot{\eta}_{\alpha\beta}$ as a pseudo strain-rate, constitutive relation (8) represents a Kelvin material with an isotropic neo-Hookean material of Young's modulus $Y(1 - \chi)$ and Poisson's ratio ν connected in parallel with a purely viscous isotropic material of bulk viscosity $\nu Y \tau / (1 + \nu)(1 - 2\nu)$ and shear viscosity $Y \tau / (1 + \nu)$. We note that for finite deformations, $E_{\alpha\beta}$ does not equal the strain rate.

Equation (18) implies that $\eta_{\alpha\beta}$ satisfies the ordinary differential equation

$$\tau \dot{\eta}_{\alpha\beta} + \eta_{\alpha\beta} = E_{\alpha\beta}. \quad (20)$$

Second-order constitutive relations (9) for the piezoelectric material were derived by Yang and Batra (1995) and contain terms quadratic in the electric field \mathbf{W} and the strain tensor \mathbf{E} . In these equations $c_1, c_2, \dots, e_1, e_2, \dots, \lambda_1, \lambda_2, \dots$ and ν_1, ν_2, \dots are material parameters. There is not sufficient test data available to evaluate all of these material parameters. Batra and Liang (1997) have shown that for an unconstrained PZT nonzero values of $c_1, c_2, c_3, c_4, c_5, e_1, e_2, e_3, e_4, e_5, \nu_4$ and ν_{12} yield a material response that is close to the one observed experimentally by Crawley and Anderson (1990). Tiersten (1975) has considered third order terms in \mathbf{W} and obtained a better agreement between the computed and the observed axial strain versus the applied electric field. Furthermore, the permittivity ε_0 of the free space is usually quite small so that Equation (12)₁ is simplified to $\pi = \mathbf{D}$. Accordingly, Equations (9) simplify to

$$\begin{aligned} S_{\alpha\beta} &= (2c_1 I_1 + c_3 I_2 + e_1 I_3) a_{\alpha} a_{\beta} \\ &\quad + (2c_2 I_2 + c_3 I_1 + e_2 I_3 + \nu_4 I_3^2) \delta_{\alpha\beta} \\ &\quad + c_4 (a_{\alpha} E_{\beta\gamma} a_{\gamma} + a_{\beta} E_{\alpha\gamma} a_{\gamma}) + 2c_5 E_{\alpha\beta} \\ &\quad + e_3 (a_{\alpha} W_{\beta} + a_{\beta} W_{\alpha}) + \nu_{12} W_{\alpha} W_{\beta}, \\ -D_{\alpha} &= (2\varepsilon_1 I_3 + e_1 I_1 + e_2 I_2 + 2\nu_4 I_2 I_3) a_{\alpha} \\ &\quad + 2\varepsilon_2 W_{\alpha} + 2e_3 E_{\alpha\beta} a_{\beta} + 2\nu_{12} E_{\alpha\beta} W_{\beta}. \end{aligned} \quad (21)$$

For an extension mode actuator poled in the x_3 -direction and the electric field also applied in the x_3 -direction,

$$a_\alpha = \delta_{3\alpha}, W_\alpha = W\delta_{3\alpha}, \quad (22)$$

and Equations (21) reduce to

$$\begin{Bmatrix} S_{11} \\ S_{22} \\ S_{33} \\ S_{23} \\ S_{31} \\ S_{12} \\ \hline D_1 \\ D_2 \\ D_3 \end{Bmatrix} = \begin{bmatrix} 2(c_2 + c_5) & 2c_2 & 2c_2 + c_3 & 0 & 0 & 0 & e_2 \\ 2c_2 & 2(c_2 + c_5) & 2c_2 + c_3 & 0 & 0 & 0 & e_2 \\ c_3 + 2c_2 & c_3 + 2c_2 & A_e & 0 & 0 & 0 & B_e \\ 0 & 0 & 0 & c_{4/2} + c_5 & 0 & 0 & 0 \\ 0 & 0 & 0 & 0 & c_{4/2} + c_5 & 0 & 0 \\ 0 & 0 & 0 & 0 & 0 & c_5 & 0 \\ \hline 0 & 0 & 0 & 0 & -e_3 & 0 & -2\nu_{12}E_{13} \\ 0 & 0 & 0 & -e_3 & 0 & 0 & -2\nu_{12}E_{23} \\ -e_2 & -e_2 & -B_e & 0 & 0 & 0 & -C_e \end{bmatrix} \times \begin{Bmatrix} E_{11} \\ E_{22} \\ E_{33} \\ 2E_{23} \\ 2E_{31} \\ 2E_{12} \\ \hline W \end{Bmatrix} + W^2 \begin{Bmatrix} \nu_4 \\ \nu_4 \\ \nu_4 + \nu_{12} \\ 0 \\ 0 \\ 0 \\ \hline 0 \end{Bmatrix} \quad (23)$$

where

$$A_e = 2(c_1 + c_2 + c_3 + c_4 + c_5), \quad B_e = e_1 + e_2 + 2e_3, \\ C_e = 2(\nu_4 E_{\gamma\gamma} + \nu_{12} E_{33}) + 2(\epsilon_1 + \epsilon_2).$$

When the PZT actuator acts in shear mode with

$$a_\alpha = \delta_{1\alpha}, W_\alpha = W\delta_{3\alpha}, \quad (24)$$

Equations (21) become

shear mode actuator. Also for our choice of directions of the polarization vector \mathbf{a} and the electric field \mathbf{W} , terms quadratic in the electric field do not appear in expressions for shear stresses. If the polarization vector \mathbf{a} were not aligned along one of the coordinate axes, then an electric field in the thickness direction will induce both normal and shear stresses in the PZT and the actuation effect for the same electric field may be enhanced. Vidoli and Batra (2000, 2001) have explored such possibilities and found optimum orientations of

$$\begin{Bmatrix} S_{11} \\ S_{22} \\ S_{33} \\ S_{23} \\ S_{31} \\ S_{12} \\ \hline -D_1 \\ -D_2 \\ -D_3 \end{Bmatrix} = \begin{bmatrix} A_s & 2c_2 + c_3 & 2c_2 + c_3 & 0 & 0 & 0 & 0 \\ 2c_2 + c_3 & 2(c_2 + c_5) & 2c_2 & 0 & 0 & 0 & 0 \\ 2c_2 + c_3 & 2c_2 & 2(c_2 + c_5) & 0 & 0 & 0 & 0 \\ 0 & 0 & 0 & c_5 & 0 & 0 & 0 \\ 0 & 0 & 0 & 0 & c_{4/2} + c_5 & 0 & e_3 \\ 0 & 0 & 0 & 0 & 0 & c_{4/2} + c_5 & 0 \\ \hline (e_1 + e_2 + 2e_3) & e_2 & e_2 & 0 & 0 & 0 & 2\nu_{12}E_{13} \\ 0 & 0 & 0 & 0 & 0 & e_3 & 2\nu_{12}E_{23} \\ 0 & 0 & 0 & 0 & e_3 & 0 & 2(\epsilon_2 + \nu_{12}E_{33}) \end{bmatrix} \times \begin{Bmatrix} E_{11} \\ E_{22} \\ E_{33} \\ 2E_{23} \\ 2E_{31} \\ 2E_{12} \\ \hline W \end{Bmatrix} + W^2 \begin{Bmatrix} 0 \\ 0 \\ \nu_{12} \\ 0 \\ 0 \\ 0 \\ \hline 0 \end{Bmatrix} \quad (25)$$

the direction of the polarization vector of a PZT beam and a rod. Vel and Batra (2001) studied cylindrical bending deformations of an extension-shear bimorph with the axis of polarization inclined at an angle α with the vertical axis. For PZT-5A, they found that the maximum tip deflection is realized in a combined extension-shear bimorph at $\alpha \approx 20^\circ$ for span-to-thickness ratio of 10 and at $\alpha \approx 28^\circ$ when the ratio is 5. We note that even when electric potential difference is applied uniformly to the top and the bottom surfaces of the PZT layer, an electric field may also be induced in x_1 and x_2 directions by the direct piezoelectric effect. Such possibilities are incorporated in the three-dimensional analysis of the problem presented herein.

Batra (2000) has modeled finite deformations of isotropic elastic materials by four frame-indifferent constitutive relations that express a stress tensor as a linear function of an appropriate strain tensor. He found that for large simple shearing or simple extensional deformations, Equation (7) predicts a stiffening behavior in the sense that the nominal stress required to deform the body increases with an increase in the magnitude of the corresponding strain. A similar result was proved by Batra and Yu (1999) for incompressible viscoelastic materials modeled by Equation (8) with the term multiplying $E_{\gamma\gamma}(t)$ replaced by a hydrostatic pressure that cannot be determined from the history of the deformation. For the present problem, strains induced in structural elements are not large enough for the stiffening effects to play a noticeable role.

In the analysis of the problem we assume that the upper and the lower surfaces of PZT layers are electroded with electrodes of negligible thickness, and all bounding surfaces of the viscoelastic layer and the host structure are electrically insulated. Even though the viscoelastic layer and the host structure may conduct electricity, such effects are not considered herein. We note that Cheng and Batra (2000) have delineated effects of electrodes on static deformations of a hybrid laminated composite. The electric potential is prescribed on the upper and the lower surfaces of the PZT layers, and surfaces $x_1 = 0, L$ are electrically insulated. Continuity conditions at the interfaces between two dissimilar materials are

$$[T_{i\alpha}N_\alpha] = 0, [u_i] = 0, \quad (26)$$

where \mathbf{N} is an outward unit normal to the surface in the reference configuration, and $[f]$ equals the difference in the values of f on the two sides of an interface. Thus the two adjoining layers are presumed to be perfectly bonded to each other with surface tractions and displacements continuous across their common interfaces. The edge $x_1 = X_1 = 0$ of the hybrid laminated plate is

rigidly clamped, and a time harmonic tangential traction is applied only to the host structure at the edge $X_1 = L$. That is

$$u_i = 0 \text{ on the surface } x_1 = X_1 = 0,$$

$$T_{i1} = 0 \text{ on the surface } X_1 = L \text{ of the PZT}$$

and the viscoelastic layer,

$$T_{i1} = -(p_0 \sin \omega t)\delta_{i3} \text{ on the surface}$$

$X_1 = L$ of the host structure.

For times $t \leq 0$, we assume that all material points of the structure are at rest and have null displacements. Thus the lower limit of integration in Equation (8) is zero.

Because of the time harmonic load applied, the response of the structure will be periodic after initial transients have died out. We note that no such assumption is made in the analysis of the problem and deformation fields as a function of time are computed numerically by the finite element method. During one cycle of deformation, energy input into the structure is given by

$$E^{\text{in}} = \int_0^{2\pi/\omega} dt \left[\int_{A_h} (-p_0 \sin \omega t) \dot{u}_3 dA - \int_{A_p} \phi \dot{D}_3 dA \right] \quad (28)$$

Here A_h is the surface of the host structure where tangential tractions (27)₃ are prescribed, and A_p surfaces $X_3 = \text{constant}$ of the PZT layers where the electric potential is applied. Work done by internal stresses in the viscoelastic layer during a cycle of deformation can be computed from

$$W = \int_0^{2\pi/\omega} dt \int_{V_{ve}} T_{i\alpha} \dot{x}_{i,\alpha} dV = \int_0^{2\pi/\omega} dt \int_{V_{ve}} S_{\alpha\beta} \dot{E}_{\alpha\beta} dV, \quad (29)$$

where V_{ve} is the region occupied by the viscoelastic layer in the reference configuration. Since stresses in the viscoelastic layer have two parts – one in phase and the other out of phase with the velocity gradients – a part of the work done W is stored in the body and the rest is dissipated. For a linear problem involving infinitesimal deformations, these two parts of stresses can be identified, e.g., see Equation (16), and the energy dissipated per cycle per unit volume of the viscoelastic material is given by

$$W^{\text{dis}} = \frac{\pi \chi \tau}{(1 + \tau^2 \omega^2)} \frac{Y}{1 + \nu} \left[\frac{\nu}{1 - 2\nu} \varepsilon_{\gamma\gamma}^\circ \varepsilon_{\alpha\alpha}^\circ + \varepsilon_{\alpha\beta}^\circ \varepsilon_{\alpha\beta}^\circ \right],$$

which equals $2\pi/\omega$ times the strain energy density of an isotropic elastic body with strains $\varepsilon_{\alpha\beta}^\circ$ and elastic moduli

equal to the loss moduli of the viscoelastic body. However, when either material or geometric or both nonlinearities are considered, such an identification is not readily available. For infinitesimal deformations of a nearly incompressible viscoelastic body, $\nu \approx 0.5$, $\epsilon_{\gamma\gamma}^o \approx 0$ and the first term in the bracket on the right-hand side of Equation (30) is negligible as compared to the second term. Thus the energy dissipated in the viscoelastic layer is predominantly due to its shearing deformations.

In a freely vibrating structural system composed of elastic and viscoelastic members, a measure of the energy dissipated during a cycle of deformation is the relative decrease in the amplitude of vibrations or the logarithmic decrement, δ^{\ln} , defined as (Timoshenko, 1974)

$$\delta^{\ln} = \ln(u_{3(j)}^{\max} / u_{3(j+1)}^{\max}) \quad (31)$$

where $u_{3(j)}^{\max}$ is the maximum displacement of a material point in the X_3 -direction during the j th cycle of deformation. Here we have chosen the X_3 -direction since the displacement in this direction is likely to be maximum. It is clear that in a continuous body the logarithmic decrement may vary from point to point. A higher value of the logarithmic decrement implies that more of the energy stored in a freely vibrating body is dissipated during each cycle of deformation. This measure of energy dissipation is valid even when material and/or geometric nonlinearities are considered. For a nonlinear problem, the value of δ^{\ln} may depend upon the cycle j of deformation. For problems studied herein, we have set $j = 2$. Note that δ^{\ln} compares amplitudes of two successive oscillations of a system and does not compare the amplitudes of oscillations obtained with and without an ACLD treatment.

The effectiveness of activating a PZT in an ACLD treatment can be measured by either one of the following two indices:

$$I_1 = \frac{|u_{3(1)}^{\max}(\text{PZTs activated})|}{|u_{3(1)}^{\max}(\text{PZTs not activated})|}, \quad (32)$$

$$I_2 = \frac{\delta^{\ln}(\text{PZTs activated})}{\delta^{\ln}(\text{PZTs not activated})} \quad (33)$$

Higher positive values of I_1 and I_2 indicate that actuating the PZT enhances the energy dissipated in the viscoelastic layer.

FINITE ELEMENT FORMULATION OF THE PROBLEM

As noted earlier, our goal is to find x_i and ϕ from Equations (2) and (4) subject to the initial and boundary

conditions. Following Hughes (1987) a weak formulation of these equations can be written as

$$\delta_{i\alpha} \delta_{i\beta} \int_{\Omega} \rho \ddot{u}_{\alpha} v_{\beta} d\Omega = \delta_{i\alpha} \left[\int_{\partial\Omega_i} f_i v_{\alpha} dS - \int_{\Omega} T_{i\beta} v_{\alpha, \beta} d\Omega \right] \quad (34)$$

$$\int_{\Omega} D_{\alpha} \psi_{, \alpha} d\Omega = \int_{\partial\Omega_c} q \psi dS,$$

where v and ψ are smooth test functions that vanish on parts of the boundary where essential boundary conditions and the electric potential are prescribed respectively. Furthermore Ω is the region occupied by the hybrid structure, $\partial\Omega_i$ the part of the boundary where surface tractions f_i ($f_i = T_{i\alpha} N_{\alpha}$) are prescribed, and $\partial\Omega_c$ the part of the boundary where the surface charge density q ($q = D_{\alpha} N_{\alpha}$) is specified. For the present problem, $q = 0$ on $\partial\Omega_c$. When v is regarded as a virtual displacement, then the left-hand side of Equation (34) equals the virtual work of inertia forces, and the two terms on the right-hand side represent the virtual work of surface tractions and internal stresses. For the host structure and the viscoelastic layer, internal stresses $T_{i\alpha}$ depend upon the mechanical deformations but for the PZT these also depend upon the electric field. Substitution for S from (7)–(9)₁ into (6) and the result into (34), and for D or π from (9)₂ into (12) and the result into (35) yields coupled equations for the determination of mechanical displacements u and the electric potential ϕ . As stated earlier, initial displacements and velocities vanish, and the pertinent boundary conditions are given in (27) and in a few lines preceding (27).

The domain Ω is discretized into the union of 8-noded disjoint brick elements Ω_e and ensuring that each element is made of a monolithic material. This is easily achieved by placing nodes on an interface between two dissimilar materials. Whereas prescribed essential boundary conditions are to be satisfied after equations at the element level have been assembled, the interface continuity conditions (26) are satisfied during the assembly of these equations. Referring the reader to Batra and Liang (1997) for details, we note that Equations (34) and (35) yield the following set of coupled nonlinear ordinary differential-algebraic equations.

$$\begin{aligned} M\ddot{u} &= F^{\text{ext}}(t) - F^{\text{int}}(u(t), \dot{u}(t), \phi(t)), \\ P^{\text{int}}(u(t), \phi(t)) &= 0, \end{aligned} \quad (37)$$

where

$$\begin{aligned} F^{\text{ext}} &= \sum_e \int_{\Omega_e \cap \partial\Omega_i} N^T f dS \\ F^{\text{int}} &= \sum_e \int_{\Omega_e} B^T T d\Omega - \sum_c \int_{\Omega_c} B^T F S d\Omega. \end{aligned} \quad (38)$$

\mathbf{B} is the 9×24 matrix relating the deformation gradient $x_{i,\alpha} = F_{i\alpha}$ to the nodal displacements, the summation in Equation (38) extends over all elements in the mesh, \mathbf{M} is the mass matrix, \mathbf{u} the vector of nodal displacements in the hybrid structure, \mathbf{F}^{ext} is the vector of nodal forces equivalent to externally applied surface tractions, \mathbf{N} is the matrix of shape functions, and \mathbf{P}^{int} is the nodal charge vector equivalent to the internal polarization. Note that only piezoelectric elements contribute to \mathbf{P}^{int} . However, all elements contribute to \mathbf{F}^{int} . In order to avoid computing the integral of the history of the strain tensor at a material point of a viscoelastic layer, we use constitutive relation (19) for the viscoelastic layer and evaluate η at each integration point from Equation (20) which is integrated by the backward difference method. Integrals over an element, like the one on the right-hand side of Equation (38)₂, are evaluated by using the $2 \times 2 \times 2$ quadrature rule.

Substitution from (19) into (38) and the result into (36) yields

$$\mathbf{M}\ddot{\mathbf{u}} + \mathbf{K}(\mathbf{u})\eta + \bar{\mathbf{K}}(\mathbf{u})\dot{\eta} = \mathbf{F}^{\text{ext}}, \quad (39)$$

where matrices \mathbf{K} and $\bar{\mathbf{K}}$ depend upon the current values of the displacement \mathbf{u} . A possibility is to simultaneously solve nonlinear Equations (20) and (39). Here Equation (36) is integrated by the central-difference method, Equation (20) is integrated at each quadrature point by the backward-difference method, and the nonlinear algebraic Equations (37) are solved by the Newton-Raphson technique. During the solution of the problem, \mathbf{F}^{int} is evaluated from the known solution at time t_n . Within a time step values of \mathbf{F}^{int} are updated till the computed successive values of \mathbf{u} and ϕ at time t_{n+1} are within the prescribed tolerance. Since the backward-difference method is unconditionally stable, the time step is controlled by the central-difference method which is explicit and conditionally stable. For a linear problem, the central-difference method is stable (Hughes, 1987) provided that $\Delta t \leq 2/\omega_{\text{max}}$ where ω_{max} is the maximum frequency of free vibration of the discretized structure. Within each time step the nonlinear problem is solved by linearizing it around the solution at time t_n . Thus, the computed solution will be stable if $\Delta t \leq 2/\omega_{\text{max}}$. Here, we take $\Delta t = 1.8/\omega_{\text{max}}$. For a nonlinear problem the structural stiffness varies with its deformations and hence ω_{max} will be a function of time resulting in uneven time steps. We employ the following recursive relation to compute nodal values of mechanical displacements at successive times:

$$\mathbf{u}(t_{n+1}) = \Delta t_2 \left[\mathbf{M}^{-1} (\mathbf{F}^{\text{ext}}(t_{n+1}) - \mathbf{F}^{\text{int}}(t_{n-1})) \frac{\Delta t_1 + \Delta t_2}{2} + \left(\frac{1}{\Delta t_1} + \frac{1}{\Delta t_2} \right) \mathbf{u}(t_n) + \frac{\mathbf{u}(t_{n-1})}{\Delta t_1} \right], \quad (40)$$

where $\Delta t_1 = t_n - t_{n-1}$ and $\Delta t_2 = t_{n+1} - t_n$. For the hybrid laminated structure being studied, the number of nodal mechanical displacement degrees of freedom is considerably more than the number of nodal electric potentials. The aforesaid explicit/implicit technique of analyzing the problem is computationally more effective both in terms of the storage and the CPU time requirements than the purely implicit technique.

Note that the problem is being analyzed in the time domain rather than the frequency domain.

COMPUTATION AND DISCUSSION OF RESULTS

The finite element code developed by Batra and Liang (1997) was modified to include the viscoelastic material behavior. Changes made in the code were verified by comparing computed results for the forced one-dimensional deformations of a viscoelastic bar with the analytical solution of the problem. When comparing the performance of extension mode and shear mode actuators in ACLD treatments, following values were assigned to various material parameters. We will find below the optimum value of the relaxation time τ and assign to it that value.

Host structure (Aluminum):

$$E = 70.3 \text{ GPa}, \quad \nu = 0.34, \quad \rho_0 = 2700 \text{ kg/m}^3;$$

Viscoelastic layer:

$$E = 298 \text{ MPa}, \quad \nu = 0.49, \quad \chi = 0.9, \quad \rho_0 = 1105 \text{ kg/m}^3;$$

PZT material:

$$\begin{aligned} c_1 &= 23.1 \text{ GPa}, & c_2 &= 33.944 \text{ GPa}, & c_3 &= 0.1996 \text{ GPa}, \\ c_4 &= -22.535 \text{ GPa}, & c_5 &= 33.49 \text{ GPa}, \\ e_1 &= 8.67544 \text{ C/m}^2, & e_2 &= 1.85657 \text{ C/m}^2, \\ e_3 &= -9.77768 \text{ C/m}^2, \\ \epsilon_0 &= 8.8419 \times 10^{-12} \text{ C/V-m}, & \epsilon_1 &= 1.0 \times 10^{-10} \text{ C/V-m} \\ \epsilon_2 &= -17.956 \times 10^{-10} \text{ C/V-m}, \\ \nu_4 &= -0.903 \times 10^{-4} \text{ N/V}^2, & \nu_{12} &= 0.305 \times 10^{-4} \text{ N/V}^2 \\ \rho_0 &= 7.500 \text{ kg/m}^3. \end{aligned}$$

The ratio of Young's modulus for the aluminum and the instantaneous Young's modulus for the viscoelastic layer is nearly 300. Young's modulus in the longitudinal direction for the PZT also equals approximately 300 times the instantaneous Young's modulus for the viscoelastic layer. Thus for both the extension mode and the shear mode configurations, a soft viscoelastic layer is sandwiched between two rather stiff layers

Unless stated otherwise results presented and discussed below are for $\nu_4 = \nu_{12} = 0$, i.e., without the consideration of W^2 terms in Equation (21).

Determination of the Fundamental Frequency

We determine the first natural frequency of the structure with the goal of exciting it at that frequency and then annulling its vibrations. The procedure to find the first natural frequency was validated by finding the natural frequencies of a simply supported 3-layer laminated square elastic plate with each layer made of an orthotropic material; the elastic constants of the top and the bottom layers were set equal to β times those of the middle layer. The elastic constants of the middle layer are

$$C = \begin{bmatrix} 1 & 0.23319 & 0.010776 & 0 & 0 & 0 \\ 0.23319 & 0.543103 & 0.098276 & 0 & 0 & 0 \\ 0.010776 & 0.098276 & 0.530172 & 0 & 0 & 0 \\ 0 & 0 & 0 & 0.26681 & 0 & 0 \\ 0 & 0 & 0 & 0 & 0.159914 & 0 \\ 0 & 0 & 0 & 0 & 0 & 0.262931 \end{bmatrix} \text{ MPa}$$

distributed normal traction of 40 kN/m^2 in the central 4% of the surface area of the top surface of the plate. Due to the symmetry about the two centroidal axes, only a quarter of the plate was modeled. The top and the bottom layers were divided into 8-node brick elements of size $1 \times 1 \times 0.1 \text{ cm}$, and the size of the element in the middle layer equaled $1 \times 1 \times 0.4 \text{ cm}$. By using $\Delta t = 20 \mu\text{s}$, time history of the vertical displacement of the centroid of the top surface of the layered plate was computed for 1 s which was analyzed by using the fast Fourier transform (FFT) to compute the natural frequencies. The variation of the first natural frequency with β is plotted in Figure 2 along with the analytical solution of Srinivas and Rao (1970), and the natural frequency obtained from the Kirchhoff plate theory as

and the mass density of each layer was taken to be 1000 kg/m^3 . Each side of the plate equaled 10 cm , and the thickness of the middle layer equaled 0.8 cm and that of each of the top and the bottom layers equaled 0.1 cm . The plate was excited by applying a uniformly

reported by Srinivas and Rao. For each value of β , the computed fundamental frequency exceeds the analytical one by at most 4%. A finer mesh ($10 \times 10 \times 6$ elements) and normal tractions applied to a larger (16%) part of the surface area did not alter the computed natural

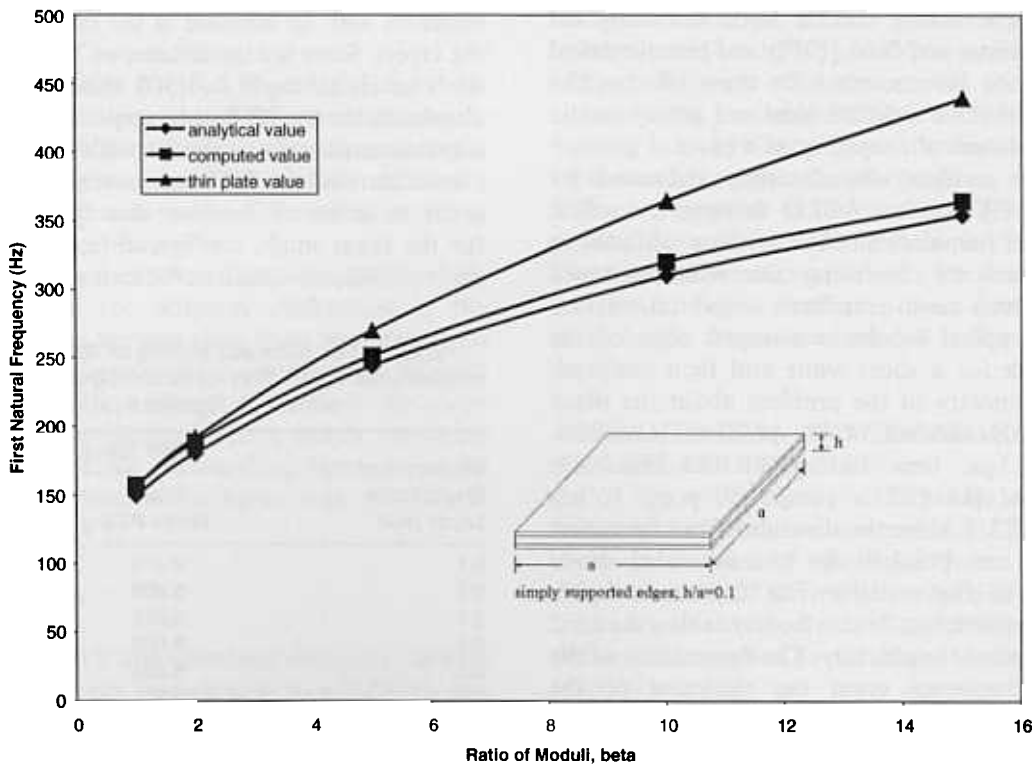


Figure 2. Comparison of the computed fundamental frequency of free vibration of a simply supported hybrid laminated plate with those obtained from the analytical solution of three-dimensional elasticity equations, and from the Kirchhoff plate theory.

frequency. Whereas for a homogeneous orthotropic plate with $\beta = 1$, the Kirchhoff plate theory gives acceptable value of the first natural frequency for the plate of aspect ratio 10, the difference between the analytical solution and that obtained from the Kirchhoff plate theory increases noticeably with an increase in the value of β . Kirchhoff's plate theory proposed for a homogeneous plate is not expected to give good results for composite laminated plates.

The classical laminated plate theory (CLPT) gives the following expression for the fundamental frequency of a simply supported rectangular laminated plate of sides a and b and thickness h .

$$= \left(\frac{\pi^2 D_{11}}{a^2 2\rho h} \right)^{1/2} \times \left[m^4 + 2 \frac{D_{12} + 2D_{66}}{D_{11}} m^2 \left(\frac{a}{b} n \right)^2 + \frac{D_{22}}{D_{11}} \left(\frac{a}{b} n \right)^4 \right]^{1/2}$$

Here D_{11} , D_{22} , D_{12} and D_{66} are the bending rigidities, and m and n are integers. For a square plate with $a/h = 10$, and $m = n = 1$, we get

$$\omega_{11}^{CLPT} = \frac{\pi}{a\sqrt{2\rho h}} [D_{11} + 2D_{12} + 4D_{66} + D_{22}]^{1/2}$$

Whereas the CLPT neglects effects of transverse shear deformations and rotary inertia, both the analytical solution of Srinivas and Rao (1970) and the numerical solution obtained here account for these effects. The consideration of shear deformations and rotary inertia lowers the fundamental frequency of a plate.

In order to analyze the damping enhanced by activating the PZTs in an ACLD treatment, we first find the natural frequencies of the systems exhibited in Figure 1(a) and (b) by using the aforementioned technique. In each case, a uniform tangential traction of 2 MPa is applied to the unclamped edge of the aluminum plate for a short while and then removed. Due to the symmetry of the problem about the plane $x_2 = 1$ cm, only one-half of the problem is studied. Using $\Delta t = 0.5 \mu s$, time history of the transverse displacement of point C is computed; point C has coordinates (15, 1, 3.5) for the shear mode configuration of Figure 1a and (15, 1, 0) for the extension mode configuration of Figure 1(b). The fundamental frequency of the system was determined by taking the FFT of the displacement time history. The dependence of the fundamental frequency upon the thickness of the viscoelastic layer is listed in Table 1. In computing these, χ in Equation (8) was set equal to 0.0; thus the energy dissipation in the viscoelastic layers was neglected. As is clear from the tabulated values, with

an increase in the thickness of each of the two viscoelastic layers from 0.1 to 1.0 cm, the fundamental frequency of the system decreases from 6.472 to 5.089 kHz for the shear mode configuration but it decreases from 9.174 to 7.791 kHz for the extension mode configuration. Note that Young's modulus in the longitudinal direction for the shear mode PZT is more than that for the extension mode PZT. Because PZT layers are farthest from the midsurface for the extension mode configuration, the effective stiffness of the extension mode configuration is more than that of the shear mode configuration. The fundamental frequencies obtained from the Euler beam theory for the shear mode and the extension mode configurations equal 18.4 and 15.1 kHz respectively for $h_{VE} = 1$ cm; however, for $h_{VE} = 0.1$ cm, each of these values equals 12.9 kHz. For $2.14 \leq L/H \leq 3$, the Euler beam theory is not expected to give good values of the fundamental frequency.

An increase in the thickness of each of the viscoelastic layers implies that either the aluminum layers or the PZT layers are located farther from the midsurface of the composite plate, and the total thickness of the plate increases. The Kirchhoff plate theory suggests that the effective stiffness of the structure will increase and thus the first natural frequency should increase with an increase in the thickness of the viscoelastic layer. However, results reported in Table 1 are in the opposite direction. As noted earlier for a plate of aspect ratio 10, the difference in the first natural frequency computed from the Kirchhoff plate theory and the analytical one increases with an increase in the ratio of the moduli of the layers. Since the instantaneous Young's modulus for the viscoelastic layer is 1/300 times that of either the aluminum or the PZT, it is very likely that the vertical displacements of similarly situated points in the aluminum and the PZT layers are loosely coupled. In order to delineate this, we have plotted in Figure 3, for the shear mode configuration, the time history of the normalized relative difference in the transverse

Table 1. For different values of the thickness of the viscoelastic layer, first natural frequency of the systems shown in Figures 1(a) and (b).

Thickness of the Viscoelastic Layer (cm)	First Natural Frequency (kHz)	
	Shear Mode PZT	Extension Mode PZT
0.1	6.472	9.174
0.2	5.906	8.734
0.3	5.655	8.482
0.4	5.529	8.294
0.5	5.404	8.168
0.6	5.341	8.074
0.7	5.278	7.980
0.8	5.215	7.917
0.9	5.152	7.854
1.0	5.089	7.791

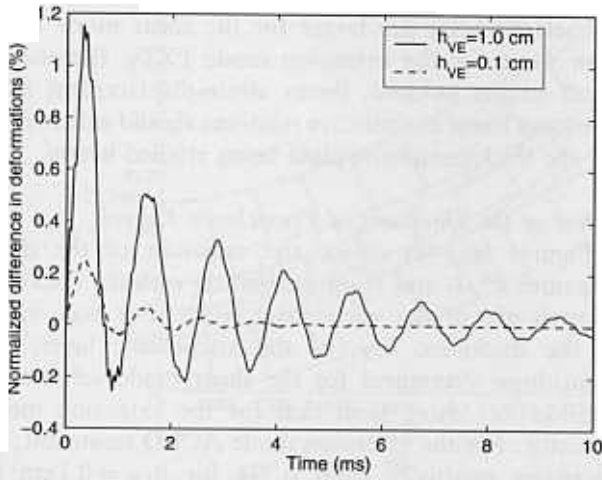


Figure 3. Time history of the normalized difference between the transverse displacements of the tips of the aluminum and the PZT layers for two values of the thickness of the intervening viscoelastic layer.

Table 2. First natural frequency of the system of Figure 1(a) for different thickness of each viscoelastic layer and for different values of the shear modulus.

Thickness of each Viscoelastic Layer (cm)	First Natural Frequency in kHz for Shear Modulus (GPa) Equal to				
	0.1	0.3	1	3	10
0.1	7.854	9.174	9.927	10.304	10.304
0.4	6.597	8.294	9.865	11.058	11.058
0.7	6.220	8.043	9.990	11.750	11.750
1.0	6.032	7.854	10.053	12.315	12.315

displacements of points D (15, 1, 0) and C (15, 1, 2.5+ h_{VE}) where h_{VE} is the thickness of the viscoelastic layer. It is clear that this difference increases with an increase in h_{VE} . However, the maximum value of this difference is less than 1.2%. Therefore, the different layers move together in the vertical direction.

We determined the first natural frequency of the shear mode configuration for different thicknesses of the viscoelastic layers by varying their shear modulus from 0.1 to 10 GPa; these results are summarized in Table 2. It is evident from these values that when the shear modulus of the viscoelastic layer is nearly one-tenth (or more) of that of the surrounding layers, then the computed natural frequencies agree with the trends predicted by the CLPT.

Analysis of Damping

We now set $\chi = 0.9$ and scrutinize damping induced by the ACLD treatment. In each case, $p_o = 0.2$ MPa and ω in Equation (27) equals the first natural frequency of the system listed in Table 1. Because of the nonzero value of χ , the first natural frequency of the composite plate will be slightly different from that listed in Table 1.

Table 3. Variation of the logarithmic decrement with the relaxation time of the viscoelastic layer.

Relaxation Time τ	Logarithmic Decrement δ
$0.25/\omega_1$	0.1918
$0.5/\omega_1$	0.3134
$1/\omega_1$	0.3688
$2/\omega_1$	0.271
$4/\omega_1$	0.1574

The load is applied for $0 \leq t \leq \pi/\omega$ and equals zero for $t \geq \pi/\omega$. For the extension mode actuators with PZTs poled in the x_3 -direction, the voltage applied to the upper surface of the top PZT layer and the lower surface of the bottom PZT layer equals the smaller of $4 \times 10^8 |u_3^C| V$ and 5 kV for $u_3^C > 0$ and the other surfaces of the PZT layers are grounded. Here u_3^C equals the transverse displacement of point C (cf. Figure 1) in meters. For $u_3^C < 0$, the voltage given by $\min\{4 \times 10^8 |u_3^C|, 5 \text{ kV}\}$ is applied to the lower surface of the top PZT layer and the upper surface of the bottom PZT layer and the other surfaces of the PZT layers are grounded. Numerical experiments gave the optimum value of the gain factor to be 4×10^8 V/m. For the shear mode PZT actuator poled in the x_1 -direction, the electric potential applied to its lower surface equals the minimum of $4 \times 10^8 |u_3^C|$ and 10 kV with the upper surface grounded when $u_3^C > 0$. For $u_3^C < 0$, the lower surface of the PZT is grounded and the voltage equal to $\min\{4 \times 10^8 |u_3^C|, 10 \text{ kV}\}$ is applied to its upper surface. We note that the electric strength of most commercially available PZTs is 2 kV/mm, and we are limiting it to 1 kV/mm. Since the thickness of the PZT layer is much smaller than its length, a uniform voltage difference applied to its surfaces $x_3 = \text{constant}$ will produce a uniform electric field in the x_3 -direction. However, deformations of the PZT layer will also induce an electric field. Both the direct and the converse piezoelectric effects are included in the analysis of the problem.

DETERMINATION OF THE OPTIMUM VALUE OF THE RELAXATION TIME

For $h_{VE} = 1.0$ cm, $\omega_1 = 5.089$ kHz and the ACLD treatment with the shear mode PZT arrangement, computed values of the logarithmic decrement for different values of the relaxation time of the viscoelastic layer are listed in Table 3. Note that no voltage difference is applied to the major surfaces of the PZT layer.

Thus, as stated above in lines preceding Equation (18), energy dissipated in the viscoelastic layer and hence the logarithmic decrement is maximum when $\tau = 1/\omega_1$ for the system excited at the fundamental frequency.

DETERMINATION OF THE OPTIMUM VALUE OF χ

With $\tau = 1/\omega_1$, we then varied χ between 0.9 and 0.5. Values of the logarithmic decrement so obtained are listed in Table 4. It is clear from these values that δ^{ln} decreases monotonically with a decrease in the value of χ . Henceforth we took $\chi = 0.9$ and $\tau = 1/\omega_1$ for both the shear mode and the extension mode ACLD treatments.

COMPARISON OF DAMPING INDUCED BY THE SHEAR MODE AND THE EXTENSION MODE ACTUATORS

Figures 4(a) and (b) depict for the shear and the extension mode configurations and $h_{VE} = 1$ cm the time history of the transverse deflection of point *C* with and without the activation of the PZTs. It is clear that in each case the transverse deflection of point *C* decreases faster when an electric potential difference is applied across the faces of the PZT layers. Also, the time periods are shortened by the actuation of the PZTs and the decrease in the time period is more for the shear mode than that for the extension mode configurations. For the same intensity of the tangential traction applied at the unclamped edge for $0 < t < \pi/\omega_1$, the transverse displacement of point *C* for the shear mode configuration is more than twice of that for the extension mode configuration. Because of the difference in the values of ω_1 for the two configurations, the impulse imparted to the shear mode configuration is 1.53 times that given to the extension mode configuration. Also, values of the first natural frequency listed in Table 1 suggest that the effective stiffness of the extension mode configuration is higher than that of the shear mode one.

In Figures 5(a) and (b) we have plotted the deformed shapes at times $t = 635$ and $1935 \mu\text{s}$ respectively of the composite plate for the shear mode PZTs, and in Figure 5(c) and (d) at $t = 410$ and $1245 \mu\text{s}$ for the extension mode PZTs. In each case displacements have been magnified by 1000 to clearly show the deformations of the viscoelastic layer. The times correspond to the instants of the first and the second maximum upward vertical displacements of point *C*. In each of the corresponding figures, shearing deformations of the

viscoelastic layer are larger for the shear mode PZTs than those for the extension mode PZTs. Because of small strains induced, linear strain-displacement relations and linear constitutive relations should suffice even for the thick composite plate being studied herein.

Effect of the Thickness of Viscoelastic Layers

Figures 6(a)–(c) evince the variation of the three measures δ^{ln} , I_1 and I_2 , of dissipation with the thickness of each one of the viscoelastic layers. For each value of the thickness, h_{VE} , of the viscoelastic layer, the logarithmic decrement for the shear mode actuator is considerably more than that for the extension mode actuator. For the extension mode ACLD treatment, δ^{ln} decreases gradually from 0.394 for $h_{VE} = 0.1$ cm to 0.243 for $h_{VE} = 1.0$ cm, but for the shear mode ACLD treatment, δ^{ln} decreases rapidly from 0.812 to 0.638 when h_{VE} is increased from 0.1 to 0.2 cm but from 0.375 to 0.367 when h_{VE} is increased from 0.9 to 1.0 cm. This is because the maximum shear strain induced in the

Table 4. Variation of the logarithmic decrement with the factor χ in the constitutive relation for the viscoelastic material.

χ	δ^{ln}
0.9	0.3688
0.8	0.3198
0.7	0.2736
0.6	0.2296
0.5	0.1875

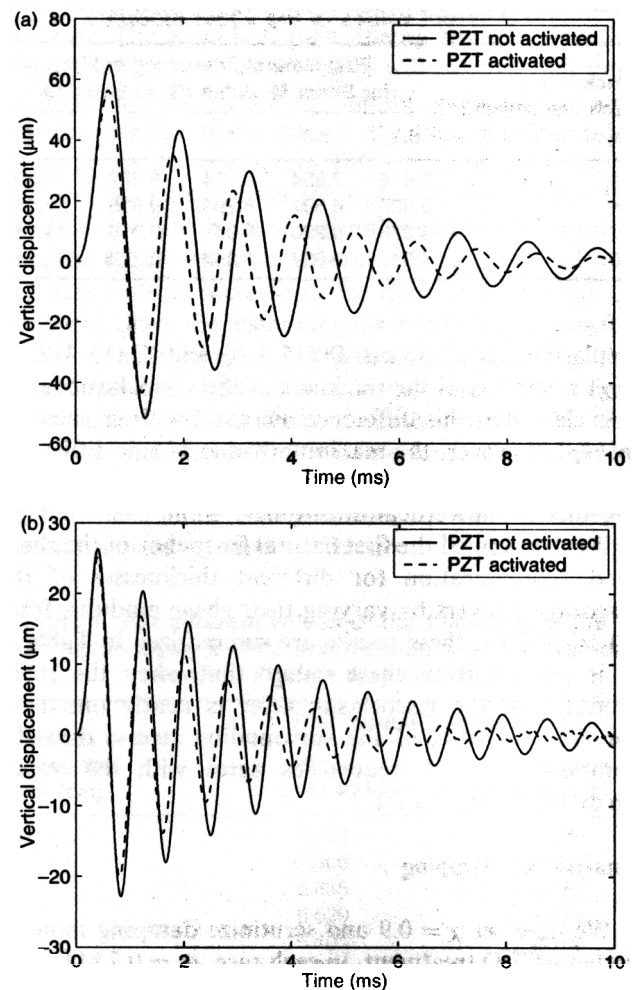


Figure 4. Time histories of the transverse displacement of point *C* with and without the application of an electric potential difference across the faces of the PZT layers: (a) shear mode configuration; (b) extension mode configuration.

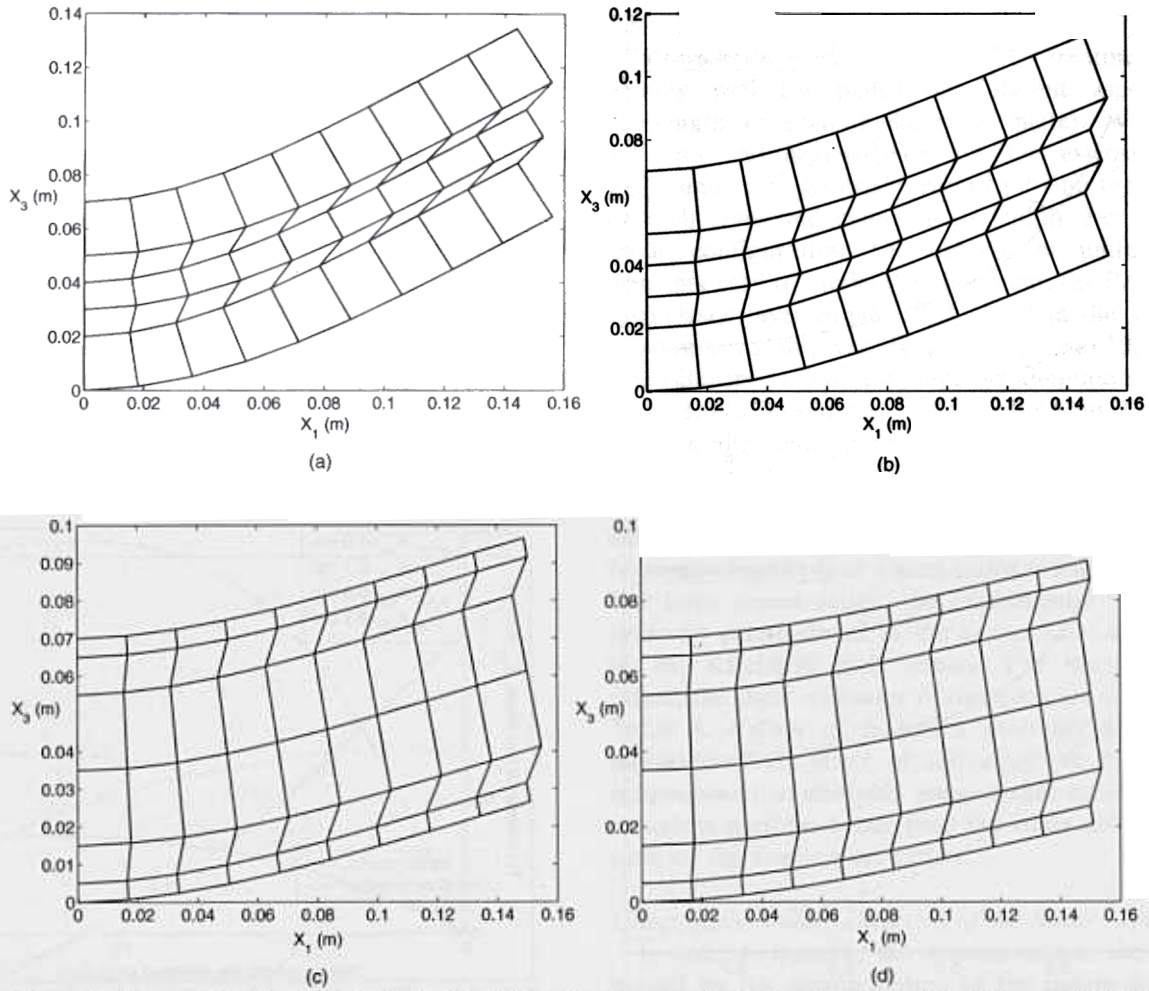


Figure 5. Deformed shapes of the laminated hybrid plate: (a) for the shear mode PZT configuration at $t = 635 \mu s$, and (b) $t = 1935 \mu s$, displacements have been magnified by a factor of 1000; (c) for the extension mode PZT configuration at $t = 410 \mu s$, and (d) $t = 1245 \mu s$, displacements have been multiplied by 1000.

viscoelastic layer decreases rapidly when h_{VE} is increased from 0.1 to 0.2 cm but slowly for subsequent increase in the values of h_{VE} ; it will be verified below. We recall that δ^n does not indicate the improvement in damping caused by the activation of the PZTs but values of I_1 and I_2 signify this effect. Whereas I_1 has a simple interpretation, I_2 does not. Both for the shear and the extension mode actuators, I_1 decreases monotonically with an increase in the thickness of each viscoelastic layer. For each one of the ten values of h_{VE} considered, I_1 for the shear mode PZT actuator is higher than that for the extension mode PZT actuator. Thus shear mode PZTs are more effective in enhancing the shearing deformations of the viscoelastic layer which in turn increase the energy dissipation and the damping of vibrations of the system. However, I_2 attains a maximum value for $h_{VE} \approx 0.3$ cm for both the extension mode and the shear mode ACLD treatment.

We have plotted in Figures 7(a) and (b) the longitudinal variation of the transverse shear strain in the viscoelastic layer for $h_{VE} = 0.1, 0.4, 0.7$ and 1.0 cm. In

each case, the transverse shear strain monotonically increases from its lowest value in the element abutting the clamped edge to the maximum value near the midspan and stays uniform from there till the free edge of the plate. Also, the maximum transverse shear strain induced in the viscoelastic layer is largest for the thinnest layer. For the shear mode actuator, the maximum value of the transverse shear strain for $h_{VE} = 0.1$ cm is 2.3 times that for $h_{VE} = 0.4$ cm; for $h_{VE} = 0.1$ cm, the maximum transverse shear strain equals 0.28%. Thus the energy dissipated per unit volume will be highest for $h_{VE} = 0.1$ cm. Since the volume of the viscoelastic material is directly proportional to h_{VE} , the total energy dissipated per cycle of vibration need not be maximum for $h_{VE} = 0.1$ cm.

Effect of the Thickness of PZT Layers

We take $h_{VE} = 0.3$ cm and study the effect on damping of the thickness of the PZT layers. For the extension mode actuator configuration, the fundamental natural frequency for $h_{PZT} = 0.1, 0.2, 0.3, 0.4$ and 0.5 cm was found to be 9.479, 9.236, 8.985, 8.734 and 8.482 kHz.

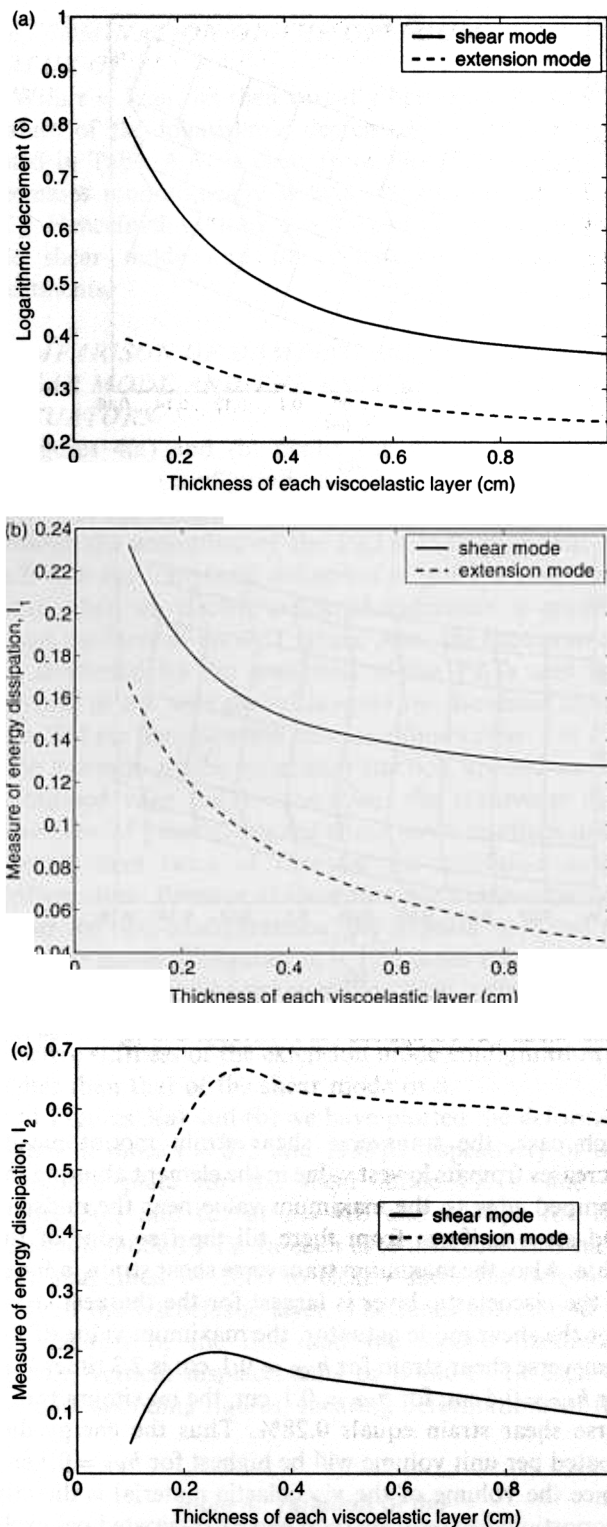


Figure 6. Dependence of the three measures of energy dissipation: (a) δ^{in} ; (b) I_1 ; (c) I_2 , upon the thickness of each one of the two viscoelastic layers.

respectively. Recalling that the thickness of the shear mode PZT actuator is twice that of each of the extension mode actuators, the corresponding natural frequency for the shear mode PZT set-up was found to be 6.220,

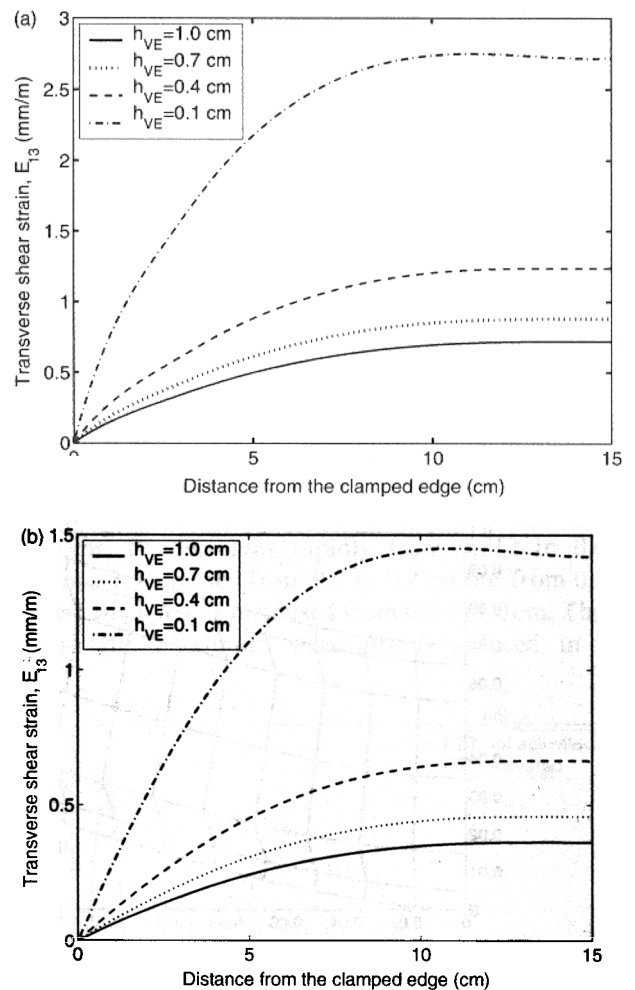


Figure 7. For four values of the thickness of the viscoelastic layers, variation of the transverse shear strain, E_{13} , on the midsurface of a viscoelastic layer: (a) shear mode actuators; (b) extension mode actuators.

6.005, 5.843, 5.718 and 5.655 kHz. As stated earlier, in each case the system was excited by tangential tractions whose frequency equals the natural frequency of the system. The dependence of the three measures of energy dissipation or damping, δ^{in} , I_1 and I_2 , upon the thickness of the PZT layer is exhibited in Figure 8(a)–(c) for the shear mode and the extension mode actuators. The electric energy input into the PZTs is different in each case. For the shear mode actuator, the logarithmic decrement has the maximum value for $h_{PZT} \approx 0.85$ cm, but for the extension mode configuration, the maximum value of δ^{in} occurs for $h_{PZT} > 1$ cm. However, for the same thickness of the PZT layers, the logarithmic decrement is higher for the shear mode configuration than that for the extension mode one. Whereas the index I_1 for the shear mode configuration increases monotonically and quite rapidly with an increase in the thickness of the PZT layer, for the extension mode configuration it attains a maximum value for $h_{PZT} \approx 0.8$ cm. The thickness of the PZT layer has a minimal

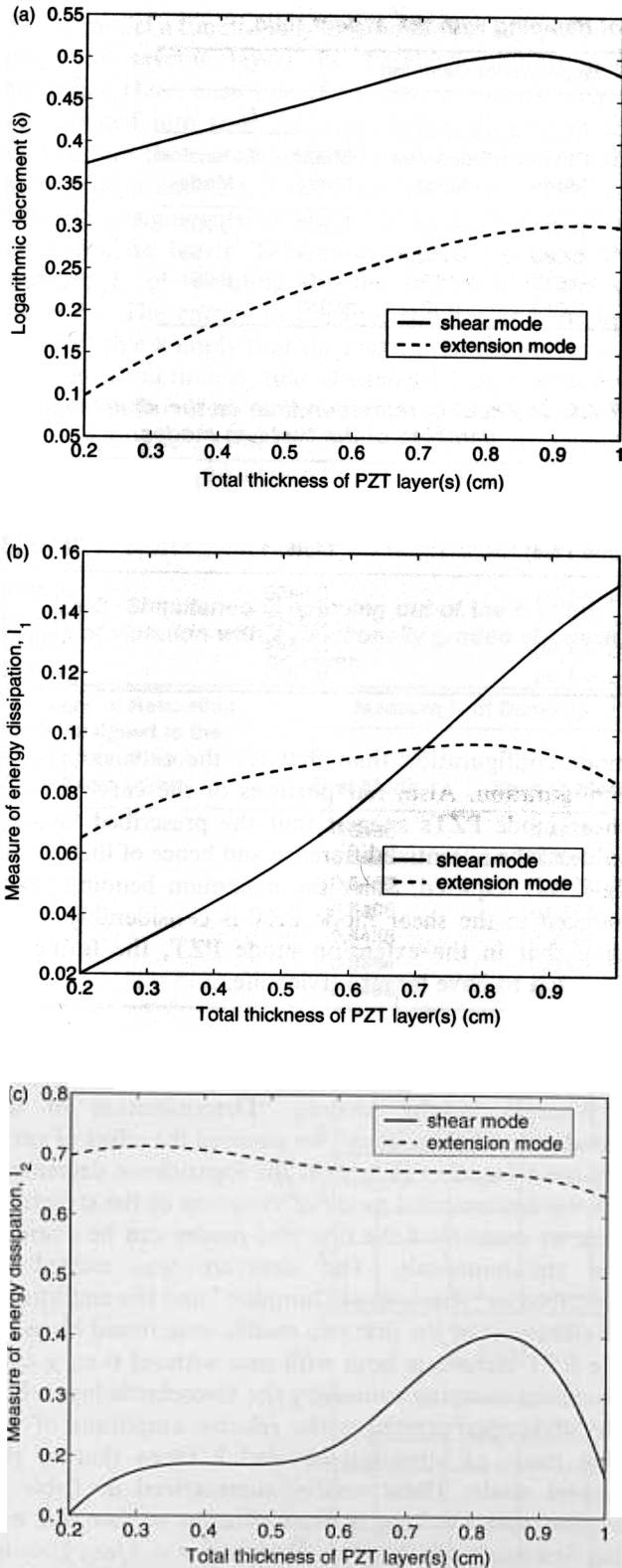


Figure 8. Dependence of the three measures of energy dissipation upon the thickness of the PZT layer: (a) δ ; (b) I_1 ; (c) I_2 .

influence on I_2 for the extension mode configuration but affects noticeably the value of I_2 for the shear mode configuration. For the shear mode configuration, the maximum value of I_2 occurs for $h_{PZT} \approx 0.8$ cm.

Effect of the Aspect Ratio of the Plate

We now explore if an ACLD treatment works equally well for plates of different aspect ratios ($s = \text{length of plate}/\text{thickness of plate}$). We set $h_{VE} = 0.3$ cm and $h_{PZT} = 0.4$ cm for the extension mode PZTs and vary the aspect ratio by fixing the thickness of each layer and changing its length. For the shear mode configuration, the number of uniform finite elements used to model the aluminum, the PZT and the viscoelastic layer equaled 9, 1 and 1 in the x_1 , x_2 and x_3 directions respectively for $s = 3$ and 10. For the extension mode configuration, the aluminum layer was divided into 2 elements in the x_3 direction. For $s = 20$ and 30, the number of elements in the longitudinal direction in each of the layers was increased to 18 and 27 respectively for both set-ups. For the shear and the extension mode configurations, the fundamental frequency for the four aspect ratios is listed in Table 5. For large aspect ratios, the fundamental frequency is inversely proportional to the aspect ratio as predicted by the Kirchhoff plate theory. For the four aspect ratios, the three measures of damping are also listed in Table 5. Values of I_1 which probably are a better indicator of the effect of activating the PZTs on the enhancement in damping suggest that extension mode actuators perform better than the shear mode ones for each of the four aspect ratios.

Effect of the Poling Direction of the Shear Mode PZT

In order to quantify the deterioration in the damping caused by the misorientation of the poling direction \mathbf{a} for the shear mode PZT, we ascertained the effect of changing \mathbf{a} in the x_1 - x_3 plane. Let \mathbf{a} make an angle θ° counterclockwise from the x_1 -axis, i.e., $\mathbf{a} = (\cos \theta, 0, \sin \theta)$. Material properties of the PZT with respect to the global axes are obtained from Equations (21). For seven values of θ , Table 6 lists the computed fundamental frequencies and the three measures of damping. Whereas the logarithmic damping is unaffected by the change in θ , values of I_1 and I_2 decrease as θ increases. Both I_1 and I_2 drop by about 10% when poling direction is inclined at 15° instead of 0° to the x_1 -axis. Thus it is important that the shear mode PZT be poled correctly for optimum performance.

We did not perform a similar study for the extension mode PZT.

Energy of Electrical Deformations

Figure 9 exhibits the time history of the energy, E_{el} , of electric deformations for the shear mode and the extension mode ACLD treatments with $h_{VE} = 1.0$ cm and $h_{PZT} = 1.0$ cm. E_{el} is defined as

$$E_{el} = \int_{\Omega_{PZT}} D_i W_i d\Omega$$

Table 5. Variation of the three measures of damping with the aspect ratio.

Aspect Ratio	Fundamental Frequency (kHz)		Measures of Damping					
	Shear Mode	Extension Mode	δ		I_1		I_2	
			Shear Mode	Extension Mode	Shear Mode	Extension Mode	Shear Mode	Extension Mode
3	6.005	9.236	0.418	0.185	0.044	0.083	0.187	0.707
10	1.165	1.257	0.374	0.055	0.082	0.258	0.009	1.155
20	0.503	0.503	0.235	0.022	0.032	0.17	0.014	0.691
30	0.314	0.314	0.153	-	0.017	0.12	0.013	-

Table 6. For the shear mode PZT, dependence upon the poling direction of the fundamental frequency and the three measures of damping.

Poling Angle θ°	Fundamental Frequency (kHz)	Measures of Damping		
		δ	I_1	I_2
0	5.089	0.369	0.128	0.092
15	5.119	0.369	0.099	0.08
30	5.129	0.367	0.053	0.025
45	5.134	0.367	0.008	-0.014
60	5.128	0.368	-0.019	-0.035
75	5.117	0.369	-0.025	-0.051
90	5.111	0.370	-0.019	-0.033

Table 7. Effect of relaxation time on the simultaneous damping of the first two modes.

Relaxation Time τ (μ s)	Measure I_1 of Damping	
	Mode 1	Mode 2
$\tau_1 = 1/\omega_1$	0.6406	0.4818
$\tau_2 = 1/\omega_2$	0.3815	0.8909
$\tau_3 = 1/\omega_3$	0.1644	0.9682
$\tau_4 = 1/\omega_4$	0.1315	0.9682

mode configuration than that for the extension mode configuration. Also, flat portions of the curve for the shear mode PZTs suggest that the prescribed limiting value of the potential difference and hence of the electric field was required. Since the maximum bending stress induced in the shear mode PZT is considerably lower than that in the extension mode PZT, the former is expected to have larger service life.

Simultaneous Damping of First Two Frequencies by Using a Functionally Graded Viscoelastic Layer

Whereas in the section, "Determination of the Fundamental Frequency" we assessed the effect of varying the relaxation time τ on the logarithmic decrement for the fundamental mode of vibration of the structure, here we examine if the first two modes can be damped out simultaneously. The structure was excited as described in "Analysis of Damping" and the amplitudes of vibrations of the first two modes were found by using the FFT technique both with and without (i.e., $\chi = 0$) modeling damping caused by the viscoelastic layer. For the undamped structure, the relative amplitude of the first mode of vibration equaled 8 times that of the second mode. These results, summarized in Table 7, suggest that $\tau = 1/\omega_1$ is most effective in damping out the first mode of vibration. However, $\tau = 1/\omega_2, 1/\omega_3$ or $1/\omega_4$ damps out better the second mode of vibration. For any one of these three values of τ , the first mode of vibration is not damped out quickly.

A possibility for damping out simultaneously the first two modes of vibration is to use a functionally graded viscoelastic layer with material properties varying continuously through the thickness. An approximate

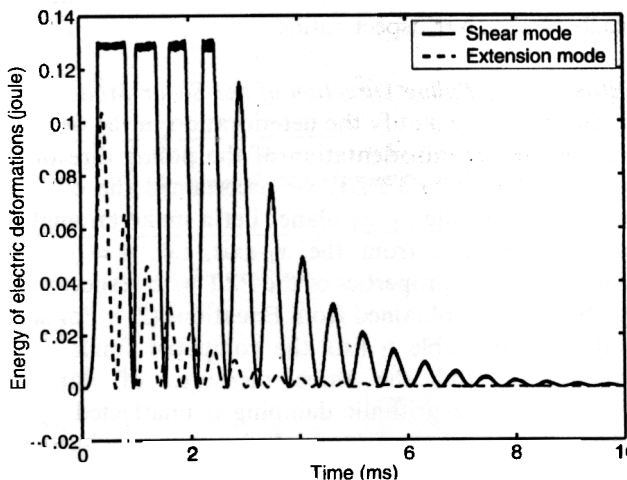


Figure 9. Time history of the energy of electric deformations for the shear mode and the extension mode ACLD treatments; $h_{VF} = 1.0$ cm, $h_{PZT} = 1.0$ cm.

where Ω_{PZT} is the region occupied by the PZT. Since a uniform electric potential is applied across the major surfaces, $x_3 = \text{constant}$, of the PZTs, only W_3 and D_3 have significant values; computed values of W_1 and W_2 were found to be several orders of magnitude lower than those of W_3 . Recall that the time periods of the two configurations are different. Larger values of the energy of electric deformations for the shear mode PZTs suggest that the potential difference imposed across the major faces of the PZT layers is higher for the shear

way to model a functionally graded layer is to consider it made of several layers of different homogeneous materials. Here, each one of the two viscoelastic layers was divided into four sublayers; when moving in the x_3 -direction these are numbered as 1, 2, 3 and 4 for the bottom layer and 4, 3, 2 and 1 for the top layer. For six different assignments of the relaxation times to these sublayers, we list in Table 8 computed values of the measure I_1 of damping for the first two modes of vibration. The entries in the first column and the last row of Table 8 imply that the material of the sublayer 1 had relaxation time τ_1 , that of sublayer 2 had relaxation time τ_2 etc. It is clear from these results that the rate of damping of the second mode of vibration is virtually unaffected by the relaxation time assigned to each of the sublayers. Since the amplitude of the first mode of vibration is 8 times that of the second mode, it may be

desirable to use homogeneous viscoelastic layers with relaxation time $\tau = 1/\omega_1$. However, the arrangement of the second row of Table 8 doubles the values of I_1 for the second mode of vibration while lowering it only about 15% for the first mode. This may be more effective in damping out quickly the total energy of a structure.

Effect of Material Nonlinearities in the Constitutive Relation for the PZT

We now investigate the effect of assigning values listed in (43) to material parameters ν_4 and ν_{12} in the constitutive relation (21) for the PZT. For each one of the ten values of the thickness of the viscoelastic layer listed in Table 1 and for the shear mode and the extension mode configurations, it was found that the value of the index I_1 was nearly the same as that for the case when $\nu_4 = \nu_{12} = 0$. For the shear mode configuration, the index I_1 was computed by considering transverse displacements of a point on the free edge of the PZT layer rather than that of a point on the aluminum layer. Figure 10 compares deformed shapes of the portion of the plate near the unclamped edge when ν_4 and ν_{12} are nonzero with those for $\nu_4 = \nu_{12} = 0$. Displacements have been magnified 100 times to clearly show the deformations. It is clear that for the extension mode configuration, the transverse shear strain in the viscoelastic layer is noticeable. The deformed shape for the shear mode configuration cannot be compared with the corresponding deformed shape for the extension mode configuration since the maximum deformations of

Table 8. Simultaneous damping out of the first two modes of vibration with a functionally graded viscoelastic layer.

Sequence of Relaxation Times Assigned to the 4 Sublayers of each Viscoelastic Layer	Measure I_1 of Damping	
	First Mode	Second Mode
1-1-1-1		
1-1-2-2		
2-2-1-1		
1-2-2-1		
2-1-1-2		
1-2-3-4		
4-3-2-1		

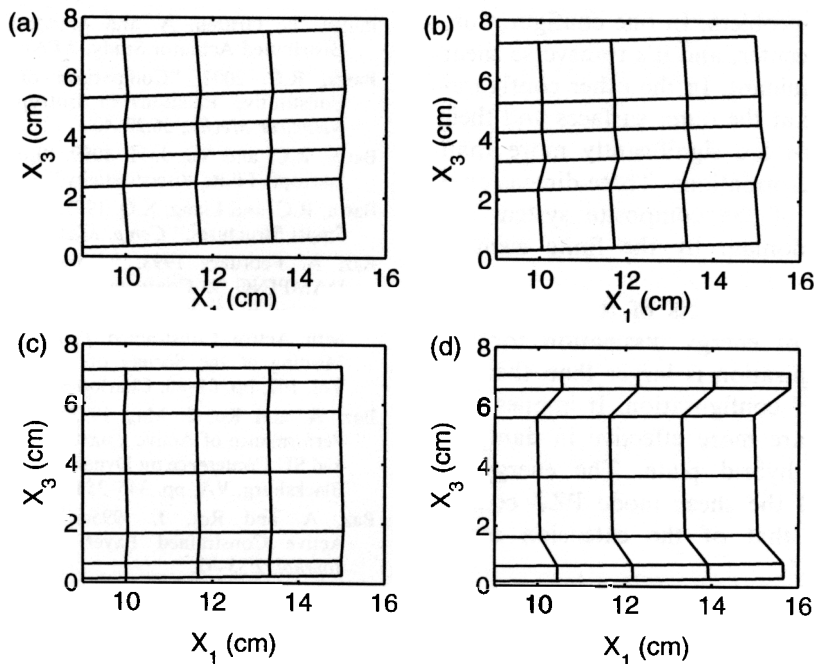


Figure 10. Deformed shapes of the laminated hybrid plate: (a) and (b) for the shear mode configuration with zero and nonzero values of ν_4 and ν_{12} ; (c) and (d) for the extension mode configuration with zero and nonzero values of ν_4 and ν_{12} .

the viscoelastic layer may not occur at the instants deformed shapes are plotted in Figure 10.

Remarks

One can improve the agreement between experimental and computed results by incorporating more terms involving different relaxation times on the right-hand side of the constitutive relation (8) for the viscoelastic layer. The consideration of each additional relaxation time will add an equation like (20) and thus increase the computational effort required to analyze the problem. One can economize on the computational effort by integrating Equation (20) only at the centroid of an element thereby tacitly assuming that $\eta_{\alpha\beta}$ is uniform over the element. This approximation is quite reasonable for a fine mesh. This generalization, though straight forward, has not been implemented in the code yet. Another extension of the work is to incorporate the effect of heat produced by electric and viscous dissipation on the temperature rise and the dependence of material moduli upon the temperature. These effects will be reported in a future study.

CONCLUSIONS

We have compared the performance of two ACLD treatments in a thick laminated plate comprised of layers made of a piezoceramic (PZT) material, aluminum and a viscoelastic material. Effects of geometric nonlinearities and the dependence of stresses and electric displacements upon squares of the electric field are incorporated into the analysis of the problem. In one configuration, the PZT layer is at the center, and its transverse shear deformations are predominant. In the other configuration, the PZT layers are at the outer surfaces and their extensional deformations are significantly more than their transverse shear deformations. Three-dimensional transient deformations of the composite system are analyzed in the time domain by the finite element method.

For each value of the thickness of the viscoelastic layer, the measure I_1 of energy dissipation for the shear mode PZT configuration is larger than that for the extension mode PZT configuration. It implies that the shear mode PZTs are more effective in damping out vibrations of the hybrid plate. The energy of electric deformations of the shear mode PZT configuration is more than that of the extension mode configuration.

The maximum transverse shear strain induced in the viscoelastic layer increases with a decrease in its thickness. The optimum thickness of the viscoelastic layers for maximum total energy dissipation is the same for each set-up. The thickness of the PZT layer which

results in the maximum value of the index I_1 of energy dissipation is the same for the two set-ups. Both arrangements result in the largest value of I_1 for a plate of aspect ratio 10. When each viscoelastic layer was divided into four sublayers and values of the relaxation moduli of the sublayers were changed between 0.1 and 0.4 times their instantaneous values, the value of the logarithmic decrement was essentially unaffected. With the objective of simultaneously damping out quickly the first two modes of vibration, each of these four sublayers was assigned a relaxation time equal to the reciprocal of the first four frequencies. These numerical experiments reveal that subdividing each viscoelastic layer into two sublayers and assigning relaxation times equal to the reciprocal of the first two frequencies to these sublayers will damp out rapidly the first two modes of vibration.

ACKNOWLEDGMENT

The work was partially supported by the NSF grant CMS9713453 and the ARO grant DAAG55-98-1-0030 to Virginia Polytechnic Institute and State University.

REFERENCES

- Azvine, B., Tomlinson, G. and Wynne, R. 1994. "Initial Studies into the Use of Active Constrained-Layer Damping for Controlling Resonant Vibrations." In: Johnson, C. (Ed.), *Proceedings of Smart Structures and Materials Conference on Passive Damping*, Orlando, Florida. Vol. 2193, pp. 138-149.
- Bailey, T., Gruzen, A. and Madden, P. 1988. RCS/Piezoelectric Distributed Actuator Study, AFAL-TR-88-038.
- Batra, R.C. 2001. "Comparison of Results from Four Linear Constitutive Relations in Isotropic Finite Elasticity," *Int. J. Nonlinear Mech.*, 36:29-40.
- Batra, R.C. and Yu, J.-H. 1999. "Linear Constitutive Relations in Isotropic Finite Viscoelasticity," *J. Elasticity*, 55:73-77.
- Batra, R.C. and Liang, X.Q. 1997. "Finite Dynamic Deformations of Smart Structures," *Comp. Mech.*, 20:427-438.
- Baz, A. February 1993. "Active Constrained Layer Damping," DAMPING '93 Conference, San Francisco, CA, pp. IBB 1-23.
- Baz, A. and Ro, J. June 1993a. "Partial Treatment of Flexible Beams with Active Constrained Layer Damping," Annual Technical Meeting of the Society of Engineering Science, ASME-AMD-Vol. 167, pp. 61-80, Charlottesville, VA.
- Baz, A. and Ro, J. May 1993b. "Finite Element Modeling and Performance of Active Constrained Layer Damping," Ninth VPI and SU Conference on Dynamics and Control of Large Structures, Blacksburg, VA, pp. 345-358.
- Baz, A. and Ro, J. 1995a. "Performance Characteristics of Active Constrained Layer Damping," *Shock and Vibration Journal*, 2:33-42.
- Baz, A. and Ro, J. 1995b. "Optimum Design and Control of Active Constrained Layer Damping," *ASME Journal of Vibration and Acoustics*, 117:135-144.
- Boriseiko, V.A., Martynenko, V.S. and Ulitko, A.F. 1983. "General Theory of Thin Piezoceramic Shells," *Vestnik Kiev. Univ., Mat. i Mekh.*, 25:26-40 (in Ukrainian).

- Cheng, Z.Q. and Batra, R.C. 2000. "Three Dimensional Asymptotic Analysis of Multiple-Electroded Piezoelectric Laminates," *AIAA J.*, 38:317–324.
- Christensen, R.M. 1971. "Theory of Viscoelasticity," *An Introduction*, Academic Press, New York.
- Crawley, E.F. and Anderson, E.H. 1990. "Detailed Models of Piezoceramic Actuation of Beams," *J. Intell. Mat. Struct.*, 1:4–24.
- DiTaranto, R.A. 1965. "Theory of Vibratory Bending for Elastic and Viscoelastic Layered Finite Length Beams," *ASME Journal of Applied Mechanics*, 87:881–886.
- Edberg, D. and Bicos, A. 1992. "Design and Development of Passive and Active Damping Concepts for Adaptive Structures." In: Knowles, G. (Ed.), *Conference on Active Materials and Adaptive Structures*, IoP Publishing Ltd., Bristol, UK, pp. 377–382.
- Hughes, T.J.R. 1987. *The Finite Element Method: Linear Static and Dynamic Finite Element Analysis*, Prentice-Hall, Englewood Cliffs, NJ.
- Liao, W.H. and Wang, K.W. 1997a. "On the Active-Passive Hybrid Vibration Control Actions of Structures with Active Constrained Layer Treatments," *ASME Journal of Vibration and Acoustics*, 119:563–572.
- Liao, W.H. and Wang, K.W. 1997b. "On the Analysis of Viscoelastic Materials for Active Constrained Layer Treatments," *J. Sound and Vibration*, 207:319–334.
- Mead, D.J. and Markus, S. 1969. "The Forced Vibration of a Three-Layer, Damped Sandwich Beam with Arbitrary Boundary Conditions," *J. of Sound and Vibration*, 10:163–175.
- Nostrand, W.C. 1994. "Active Constrained Layer Damping Using PZT Actuators," PhD Dissertation, State University of New York at Buffalo.
- Plump, J. and Hubbard, J.E. 1986. "Modeling of an Active Constrained Layer Damper," Twelfth Intl. Congress on Acoustics, Paper #D41, Toronto, Canada, 24–31 July.
- Shen, I.Y. 1994. "Hybrid Damping Through Intelligent Constrained Layer Treatments," *ASME Journal of Vibration and Acoustics*, 116:341–349.
- Srinivas, S. and Rao, A.K. 1970. "Bending, Vibration and Buckling of Simply Supported Thick Orthotropic Rectangular Plates and Laminates," *Int. J. Solids and Structures*, 6:1463–1481.
- Sun, C.T. and Zhang, X.D. 1996. "Formulation of an Adaptive Sandwich Beam," *Smart Mat. and Structures*, 5:814–823.
- Tiersten, H.F. 1975. "Nonlinear Electroelastic Equations Cubic in Small-Field Variables," *J. Acoustical Soc. America*, 57:660–666.
- Timoshenko, S. 1974. *Vibration Problems in Engineering*, Butterworth, Heinemann, Oxford.
- Tzou, H.S. and Bao, Y. 1997. "Nonlinear Piezothermoelasticity and Multi-Field Actuations, Part I: Nonlinear Anisotropic Piezothermoelastic Shell Laminates," *J. Vibration and Acoustics*, 119:374–381.
- Van Nostrand, W., Knowles, G. and Inman, D. 1994. "Finite Element Modeling for Active Constrained-Layer Damping." In: Johnson, C. (Ed.), *Proceedings of Smart Structures and Materials Conference on Passive Damping*, Orlando, Florida, Vol. 2193, pp. 126–137.
- Vel, S.S. and Batra, R.C. 2001a. "Exact Solution for the Cylindrical Bending of Laminated Plates with Embedded Shear Actuators," *Smart Materials and Structures*, 10:240–251.
- Vel, S.S. and Batra, R.C. 2001b. "Exact Solution for Rectangular Sandwich Plates with Embedded Piezoelectric Shear Actuators," *AIAA J.*, 39:1363–1373.
- Vel, S.S. and Batra, R.C. 2001. "Analysis of Piezoelectric Bimorphs and Plates with Segmented Actuators," *J. Thin-Walled Structures*, 39:23–44.
- Vidoli, S. and Batra, R.C. 2000. "Derivation of Plate and Rod Equations for a Piezoelectric Body from a Mixed Three-Dimensional Variational Principle," *J. Elasticity*, 59:23–50.
- Vidoli, S. and Batra, R.C. 2001. "Coupled Extensional and Torsional Deformations of a Piezoelectric Cylinder," *Smart Materials and Structures*, 10:300–304.
- Yang, J.S. and Batra, R.C. 1995. "A Second-Order Theory of Piezoelectric Materials," *J. Acoustic Soc. America*, 97:280–288.
- Yu, J.-H. and Batra, R.C. 2000. "Constrained Layer Damping in Finite Shearing Deformations," *Journal of Sound and Vibration*, 229:445–452.
- Yu, Y.Y. 1995. "On the Ordinary, Generalized, and Pseudo-Variational Equations of Motion in Nonlinear Elasticity, Piezoelectricity, and Classical Plate Theories," *J. Applied Mechanics*, 62:471–478.
- Zhang, X.D. and Sun, C.T. 1999. "Analysis of a Sandwich Plate Containing a Piezoelectric Core," *Smart Mat. and Structures*, 8:31–40.